J|A|C|S
ARTICLES
Published on Web 06/19/2003

Rational Design Principle for Modulating Fluorescence Properties of Fluorescein-Based Probes by Photoinduced Electron Transfer

Tetsuo Miura,[†] Yasuteru Urano,[†] Kumi Tanaka,[†] Tetsuo Nagano,*[,†] Kei Ohkubo,[‡] and Shunichi Fukuzumi*[,‡]

Graduate School of Pharmaceutical Sciences, The University of Tokyo, Hongo, Bunkyo-ku, Tokyo 113-0033, Japan, and Department of Material and Life Science, Graduate School of Engineering, Osaka University, CREST, Japan Science and Technology Corporation (JST), Yamada-oka, Suita, Osaka 565-0871, Japan

Received March 22, 2003; E-mail: tlong@mol.f.u-tokyo.ac.jp; fukuzumi@ap.chem.eng.osaka-u.ac.jp

Abstract: Fluorescence properties of fluorescein-based probes are shown to be finely controlled by the rate of photoinduced electron transfer from the benzoic acid moiety (electron donor) to the singlet excited state of the xanthene moiety (electron acceptor fluorophore). The occurrence of photoinduced electron transfer is clearly evidenced by transient absorption spectra showing bands due to the radical cation of the electron donor moiety and the radical anion of the xanthene moiety, observed in laser flash photolysis experiments. The photoinduced electron transfer rates and the rates of back electron transfer follow the Marcus parabolic dependence of electron transfer rate on the driving force. Such a dependence provides for the first time a quantitative basis for a rational design principle which has high efficiency in modulating fluorescence properties of fluorescein-based probes.

Fluorescence imaging is the most powerful technique currently available for continuous observation of the dynamic intracellular processes of living cells. Fluorescein is widely employed as the core of various fluorescence probes used in imaging important biological effectors, such as nitric oxide and calcium.[1−5] Despite the extensive use of fluorescein derivatives and the importance of the applications, the mechanism that controls the quantum yield of fluorescence has not been fully established. Without such mechanistic information there can be no rational design strategy to develop new, practically useful fluorescence probes. A plausible mechanism that might control the fluorescence quantum yields of fluorescein derivatives has been suggested to be photoinduced electron transfer from the electron donor moiety to the singlet excited state of the xanthene moiety.[6] Since the fluorescence quantum yields in photoinduced electron transfer reactions may be quantitatively predicted on the basis of the Marcus theory of electron transfer,[7−9] confirmation of the above mechanism would provide a quantitative basis for rational design of fluorescence probes. Further, the stability of fluorescence probes could be increased by accelerating the back electron transfer in the radical ion pair generated by photoinduced electron transfer. The shorter the lifetime of the highly reactive intermediate state, such as the radical ion pair, the less will be the cell damage. However, the occurrence of photoinduced electron transfer in fluorescein-based probes has yet to be established.

We report herein the first definitive evidence for the occurrence of photoinduced electron transfer in fluorescein-based probes in which the electron donor moiety is directly linked with the xanthene moiety. Formation of the radical ion pair upon photoirradiation of the fluorescein-based probes was detected by means of laser flash photolysis experiments, which afforded transient absorption spectra showing bands due to the radical cation of the electron donor moiety and the xanthene radical anion. The rates of photoinduced electron transfer and the back electron transfer were determined and analyzed in terms of the Marcus theory of electron transfer. The results provide for the first time a quantitative basis for rational design of fluorescein-based probes with high efficiency in fluorescence ON/OFF switching, as well as high stability to repeated photoirradiation.

Experimental Section

Materials and General Instrumentation. General chemicals were of the best grade available, supplied by Tokyo Chemical Industries, Wako Pure Chemical, or Aldrich Chemical Co., and were used without further purification. Other chemicals used were dimethyl sulfoxide (DMSO, fluorometric grade, Dojindo) and tetrabutylammonium perchlorate (TBAP, electrochemical grade, dried over P_2O_5 before use,

[†] The University of Tokyo.
[‡] Osaka University.

(1) Minta, A.; Kao, J. P. Y.; Tsien, R. Y. *J. Biol. Chem.* **1989**, *264*, 8171−8178.
(2) Kojima, H.; Nakatsubo, N.; Kikuchi, K.; Kawahara, S.; Kirino, Y.; Nagoshi, H.; Hirata, Y.; Nagano, T. *Anal. Chem.* **1998**, *70*, 2446−2453.
(3) Umezawa, N.; Tanaka, K.; Urano, Y.; Kikuchi, K.; Higuchi, T.; Nagano, T. *Angew. Chem., Int. Ed.* **1999**, *38*, 2899−2901.
(4) Walkup, G. K.; Burdette, S. C.; Lippard, S. J.; Tsien, R. Y. *J. Am. Chem. Soc.* **2000**, *122*, 5644−5645.
(5) Hirano, T.; Kikuchi, K.; Urano, Y.; Higuchi, T.; Nagano, T. *J. Am. Chem. Soc.* **2000**, *122*, 12399−12400.
(6) Tanaka, K.; Miura, T.; Umezawa, N.; Urano, Y.; Kikuchi, K.; Higuchi, T.; Nagano, T. *J. Am. Chem. Soc.* **2001**, *123*, 2530−2536.
(7) Marcus, R. A. *Annu. Rev. Phys. Chem.* **1964**, *15*, 155−196.
(8) Marcus, R. A.; Sutin, N. *Biochim. Biophys. Acta* **1985**, *811*, 265−322.
(9) Marcus, R. A. *Angew. Chem., Int. Ed. Engl.* **1993**, *32*, 1111−1121.

10.1021/ja035282s CCC: $25.00

Fluka). Acetonitrile, acetone, *N*,*N*-dimethylformamide (DMF), tetrahydrofuran (THF), methanol, and ethanol were used after appropriate distillation or purification. NMR spectra were recorded on a JNM-LA300 (JEOL) instrument at 300 MHz for ^{1}H NMR and at 75 MHz for ^{13}C NMR. Mass spectra (MS) were measured with a JMS-DX300 (JEOL) for EI and a SX-102A (JEOL) for FAB. All experiments were carried out at 298 K, unless otherwise specified.

Preparation of 9-[1-(2-Carboxy-4-hydroxy)phenyl]-6-hydroxy-3*H*-xanthen-3-one (4-Hydroxyfluorescein). 4-Aminofluorescein (350 mg) was dissolved in 1.5 mL of sulfuric acid and 4 mL of water. To this solution was added 240 mg of sodium nitrite. After stirring at 0 °C for 2 h, 15 mg of urea was added. Sulfuric acid (0.5 mL) was diluted with 10 mL of water, and to this was added dropwise the prepared diazonium ion solution at 100 °C. The reaction mixture was refluxed for 2 h, and the resulting solid was collected by filtration. The crude product was purified by silica gel chromatography to afford 340 mg of 4-hydroxyfluorescein (yield 97.7%). ^{1}H NMR (300 MHz, DMSO-d_6): δ 6.54 (dd, 2H, J = 8.6, 2.2 Hz), 6.57 (d, 2H, J = 8.5 Hz), 6.65 (d, 2H, J = 2.1 Hz), 7.03 (d, 1H, J = 7.9 Hz), 7.16 (dd, 1H, J = 8.0, 2.4 Hz), 7.18 (d, 1H, J = 2.4 Hz). MS (EI$^+$): m/z 348 (M$^+$).

Preparation of 9-[1-(2-Carboxy-4-acetamido)phenyl]-6-hydroxy-3*H*-xanthen-3-one (4-Acetamidofluorescein). 4-Aminofluorescein (1.0 g) was suspended in 25 mL of acetic anhydride. After addition of 1 mL of pyridine, the reaction mixture was stirred at 140 °C for 1 h, then cooled to room temperature. The precipitate was filtered off and dried in vacuo to afford 1.27 g of 3′,6′-bis(acetoxy)-6-acetamidospiro-[benzo[2,3-*c*]furan-1(3*H*),9′-[9*H*]-xanthen]-3-one. The obtained compound (1.0 g) was resuspended in a mixture of methanol (50 mL), 25% aqueous ammonium solution (15 mL), and water (10 mL). The whole was stirred at room temperature for 10 min, then hydrochloric acid was added. The organic solvent was removed under reduced pressure, and the precipitate was collected by filtration and dried in vacuo. Yield: 818 mg (quant.). ^{1}H NMR (300 MHz, DMSO-d_6): δ 2.11 (s, 3H), 6.52 (dd, 2H, J = 8.6, 2.2 Hz), 6.56 (d, 1H, J = 8.6 Hz), 6.67 (d, 1H, J = 2.2 Hz), 7.19 (d, 1H, J = 8.4 Hz), 7.80 (dd, 1H, J = 8.4, 1.9 Hz), 8.29 (d, 1H, J = 1.9 Hz). MS (EI$^+$): m/z 389 (M$^+$).

Syntheses of Methylated Fluorescein Derivatives. Fluorescein and 4-aminofluorescein were purchased from Tokyo Chemical Industries. 4-Hydroxyfluorescein and 4-acetamidofluorescein were synthesized according to the aforementioned schemes. DPAX (**8**),[3] 9-[2-(3-carboxy)-naphthyl]-6-hydroxy-3*H*-xanthen-3-one (NX, **6**), and 9-[2-(3-carboxy)-anthryl]-6-hydroxy-3*H*-xanthen-3-one (AX, **7**)[6] were prepared according to the literature. All methylated fluorescein derivatives were synthesized by means of the following procedure: to a suspension of a fluorescein derivative in methanol was added a few drops of sulfuric acid. The reaction mixture was refluxed for 12 h, then poured onto ice, and extracted with CH_2Cl_2. The organic layer was dried over Na_2SO_4 and evaporated. The obtained methyl ester was dissolved in acetone. To this solution, 2 (or 3 in the case of 4-hydroxyfluorescein) equiv of iodomethane and cesium carbonate were added. The mixture was stirred for 5 h at room temperature, water was added, and the whole was extracted with CH_2Cl_2. The organic layer was dried and evaporated. The crude product was purified by silica gel chromatography to afford the pure methylated fluorescein derivative.

9-[1-(2-Methoxycarbonyl)phenyl]-6-methoxy-3*H*-xanthen-3-one (1). ^{1}H NMR (300 MHz, $CDCl_3$): δ 3.57 (s, 3H), 3.90 (s, 3H), 6.23 (d, 1H, J = 1.8 Hz), 6.38 (dd, 1H, J = 9.7, 1.8 Hz), 6.78 (d, 1H, J = 9.7 Hz), 6.82 (d, 1H, J = 8.8 Hz), 6.88 (dd, 1H, J = 8.9, 2.2 Hz), 7.21 (d, 1H, J = 2.2 Hz), 7.48 (d, 1H, J = 7.7 Hz), 7.76 (t, 1H, J = 7.7 Hz), 7.86 (t, 1H, J = 7.7 Hz), 8.20 (d, 1H, J = 7.7 Hz). MS (EI$^+$): m/z 360 (M$^+$). Mp: 206 °C.

9-[1-(2-Methoxycarbonyl-4-amino)phenyl]-6-methoxy-3*H*-xanthen-3-one (3). ^{1}H NMR (300 MHz, $CDCl_3$): δ 3.57 (s, 3H), 3.91 (s, 3H), 4.16 (br, 2H), 6.43 (d, 1H, J = 2.0 Hz), 6.55 (dd, 1H, J = 9.7, 2.0 Hz), 6.73 (dd, 1H, J = 9.0, 2.4 Hz), 6.93−7.05 (m, 5H), 7.48 (d, 1H, J = 2.4 Hz). MS (EI$^+$): m/z 375 (M$^+$). Mp: 209 °C.

9-[1-(2-Methoxycarbonyl-4-acetamido)phenyl]-6-methoxy-3*H*-xanthen-3-one (4). ^{1}H NMR (300 MHz, $CDCl_3$): δ 2.28 (s, 3H), 3.61 (s, 3H), 3.92 (s, 3H), 6.46 (d, 1H, J = 1.9 Hz), 6.50 (dd, 1H, J = 9.7, 2.0 Hz), 6.74 (dd, 1H, J = 8.8, 2.3 Hz), 6.85 (d, 1H, J = 9.7 Hz), 6.93 (d, 1H, J = 9.7 Hz), 6.95 (d, 1H, J = 2.3 Hz), 8.00 (s, 1H), 8.01 (dd, 1H, J = 8.8, 2.4 Hz), 8.31 (d, 1H, J = 2.3 Hz). MS (EI$^+$): m/z 417 (M$^+$). Mp: 233 °C.

9-[1-(2-Methoxycarbonyl-4-methoxy)phenyl]-6-methoxy-3*H*-xanthen-3-one (5). ^{1}H NMR (300 MHz, $CDCl_3$): δ 3.61 (s, 3H), 3.92 (s, 3H), 3.96 (s, 3H), 6.44 (d, 1H, J = 1.8 Hz), 6.53 (dd, 1H, J = 9.7, 1.8 Hz), 6.73 (dd, 1H, J = 9.0, 2.6 Hz), 6.88−6.95 (m, 3H), 7.18−7.24 (m, 2H), 7.73 (d, 1H, J = 2.6 Hz). MS (EI$^+$): m/z 390 (M$^+$). Mp: 215 °C.

9-[2-(3-Methoxycarbonyl)naphthyl]-6-methoxy-3*H*-xanthen-3-one (6). ^{1}H NMR (300 MHz, $CDCl_3$): δ 3.63 (s, 3H), 3.90 (s, 3H), 6.26 (d, 1H, J = 2.0 Hz), 6.35 (dd, 1H, J = 9.5, 1.9 Hz), 6.82−6.92 (m, 3H), 7.24 (d, 1H, J = 2.6 Hz), 7.75−7.81 (m, 2H), 8.05−8.11 (m, 2H), 8.26−8.30 (m, 1H), 8.90 (s, 1H). MS (EI$^+$): m/z 410 (M$^+$). Mp: 248 °C.

9-[2-(3-Methoxycarbonyl)anthryl]-6-methoxy-3*H*-xanthen-3-one (7). ^{1}H NMR (300 MHz, DMSO-d_6): δ 3.66 (s, 3H), 3.91 (s, 3H), 6.26 (d, 1H, J = 1.8 Hz), 6.37 (dd, 1H, J = 9.7, 1.8 Hz), 6.86 (dd, 1H, J = 8.8, 2.4 Hz), 6.99 (d, 1H, J = 4.7 Hz), 7.02 (d, 1H, J = 5.5 Hz), 7.25 (d, 1H, J = 2.3 Hz), 7.64−7.68 (m, 2H), 8.13−8.23 (m, 3H), 8.73 (s, 1H), 9.01 (s, 1H), 9.09 (s, 1H). MS (EI$^+$): m/z 460 (M$^+$). Mp: 290 °C.

9-[2-(3-Methoxycarbonyl-9,10-diphenyl)anthryl]-6-methoxy-3*H*-xanthen-3-one (8). ^{1}H NMR (300 MHz, $CDCl_3$): δ 3.53 (s, 3H), 3.89 (s, 3H), 6.42 (d, 1H, J = 1.8 Hz), 6.50 (dd, 1H, J = 9.7, 1.7 Hz), 6.69 (dd, 1H, J = 9.0, 2.6 Hz), 6.92 (d, 1H, J = 2.4 Hz), 6.95−7.00 (m, 2H), 7.41−7.82 (m, 15H), 8.66 (s, 1H). MS (EI$^+$): m/z 612 (M$^+$). Mp: 185 °C.

Synthesis of 6-Methoxy-3*H*-xanthen-3-one (2). To a solution of 230 mg (1.01 mmol) of 3-hydroxy-6-methoxy-9*H*-xanthene, synthesized from 2,2′,4,4′-tetrahydroxybenzophenone according to the procedure reported by Shi et al.,[10] in 9 mL of ethanol was added 2,3-dichloro-5,6-dicyano-1,4-benzoquinone (560 mg, 2.47 mmol) at room temperature. The reaction mixture was stirred for 8 h at room temperature, then 10 mL of water was added, and the whole was extracted with ethyl acetate. The organic layer was dried, then evaporated. The crude product was purified by silica gel chromatography to afford 51 mg of pure **2** (yield 22.3%). ^{1}H NMR (300 MHz, DMSO-d_6): δ 3.90 (s, 3H), 6.15 (s, 1H), 6.50 (dd, 1H, J = 9.4, 2.4 Hz), 7.02 (dd, 1H, J = 8.8, 2.5 Hz), 7.15 (d, 1H, J = 2.4 Hz), 7.55 (d, 1H, J = 9.5 Hz), 7.74 (d, 1H, J = 8.8 Hz), 8.24 (s, 1H). MS (EI$^+$): m/z 226 (M$^+$). Mp: 120 °C.

Syntheses of Benzene Moieties of Methylated Fluorescein Derivatives. The benzene moieties of methylated fluorescein derivatives, i.e., substituted methyl benzoates, were synthesized by refluxing the corresponding substituted benzoic acids in methanol with several drops of sulfuric acid. All the benzoic acid derivatives are commercially available, except 9,10-diphenyl-2-anthracenecarboxylic acid.

2-Methoxycarbonyl-9,10-diphenylanthracene. The carboxylic acid moiety of anthraquinone-2-carboxylic acid was protected with the oxazoline group according to the literature.[11] After coupling of 2-substituted anthraquinone (303 mg, 1 mmol) with phenylmagnesium bromide (1.0 mol L^{-1} THF solution, 5 mL, 5 mmol) via Grignard reaction, the generated 2-substituted 9,10-dihydro-9,10-dihydroxyanthracene (209 mg, 0.45 mmol) was aromatized with an excess amount of tin(II) chloride (3.0 g, 15.8 mmol) in a mixture of acetic acid (7.5 mL) and hydrochloric acid (3.0 mL). The oxazoline moiety was removed by hydrolysis under acidic conditions. Then, to a solution of 9,10-diphenyl-2-anthracenecarboxylic acid (40 mg, 0.11 mmol) in

(10) Shi, J. M.; Zhang, X. P.; Neckers, D. C. *J. Org. Chem.* **1992**, *52*, 4418−4421.
(11) Meyers, A. I.; Temple, D. L.; Haidukew, D.; Mihelich, E. D. *J. Org. Chem.* **1974**, *39*, 2787−2793.

methanol was added a few drops of sulfuric acid. After refluxing for 6 h, the reaction mixture was poured onto ice. After extraction with CH_2Cl_2, the crude product was purified by silica gel chromatography to afford 35 mg of pure 2-methoxycarbonyl-9,10-diphenylanthracene (yield 82.9%). ^{1}H NMR (300 MHz, $CDCl_3$): δ 3.79 (s, 3H), 7.46−7.70 (m, 15H), 7.82 (dd, 1H, J = 9.2, 1.8 Hz), 8.35 (d, 1H, J = 1.8 Hz). MS (EI$^+$): m/z 388 (M^+). Mp: 123 °C.

Fluorescence Properties and Quantum Efficiency of Fluorescence. Steady-state fluorescence spectroscopic studies were performed on an F4500 (Hitachi). UV−visible spectra were obtained on a UV-1600 (Shimadzu), with 0.1 mol L^{-1} sodium phosphate buffer (pH 7.4) as the solvent. Each solution contained up to 0.2% (v/v) DMSO as a cosolvent. For determination of the quantum efficiency of fluorescence (ϕ_f), fluorescein in 0.1 mol L^{-1} NaOH (ϕ_f 0.85) was used as a fluorescence standard.[12] The quantum efficiencies of fluorescence were obtained from multiple measurements (N = 3) with the following equation (F denotes fluorescence intensity at each wavelength and $\sum[F]$ was calculated by summation of fluorescence intensity).

$$\phi^{(\text{sample})} = \phi^{(\text{standard})} \frac{\text{Abs}^{(\text{standard})}}{\text{Abs}^{(\text{sample})}} \frac{\sum[F^{(\text{sample})}]}{\sum[F^{(\text{standard})}]}$$

Fluorescence decay of **2** was recorded with a C4780 system (Hamamatsu Photonics). The solution of **2** was prepared to be 5.0 × 10^{-6} M in 0.1 mol L^{-1} sodium phosphate buffer (pH 7.4) containing 1.0% DMSO as a cosolvent. It was excited with an N_2:Coumarin 307 pulse laser. The obtained data were appropriately deconvoluted and fitted to monoexponential decay curves to determine the fluorescence lifetime (τ_0) of **2** as 3.6 ns.

Cyclic Voltammetry. Cyclic voltammetry was performed on a 600A electrochemical analyzer (ALS). A three-electrode arrangement in a single cell was used for the measurements: a Pt wire as the auxiliary electrode, a Pt microelectrode (i.d. = 25 μm) as the working electrode, and an Ag/Ag$^+$ electrode as the reference electrode. The sample solutions contained 1.0 × 10^{-3} M sample and 0.1 M tetrabutylammonium perchlorate (TBAP) as a supporting electrolyte in acetonitrile, and argon was bubbled for 10 min before each measurement. Obtained potentials (vs Ag/Ag$^+$) were converted to those vs SCE by adding 0.29 V.

Laser Flash Photolysis. The measurements of transient absorption spectra of **8** in acetonitrile were performed according to the following procedures. The deaerated acetonitrile solution of **8** (5.0 × 10^{-5} M) was excited by a Nd:YAG laser (GCR-130, Quanta-Ray) at 475 nm with the power of 4.5 mJ. A pulsed xenon flash lamp (XF80-60, Tokyo Instruments) was used for the probe beam. The output was recorded with a digitizing oscilloscope (HP 54510B, 300 MHz).

ESR Measurements. The ESR measurements of photoexcited **8** were carried out with a JES-RE1XE X-band spectrometer (JEOL) to detect the transient radical species in a solution of **8** (1.0 × 10^{-3} M) in frozen acetonitrile at 143 K under irradiation with light from a high-pressure mercury lamp (USH-1005D, Ushio). A quartz ESR tube containing a deaerated acetonitrile solution of **8** was irradiated in the cavity of the ESR spectrometer with the focused light of a 1000 W high-pressure Hg lamp through an aqueous filter at low temperature. The ESR spectra in frozen acetonitrile were measured at 143K using an attached variable-temperature apparatus.

Results and Discussion

The structures of the fluorescein-based fluorescence probes employed in this study (**1**−**8**) are shown in Figure 1A.

Both the carboxylic acid and the phenolic moiety of the fluorescein derivatives are methylated to avoid complex pH-dependent equilibria which would affect the fluorescence quantum yields.[13] Various electron donors are directly linked with the xanthene moiety. There is little interaction between the benzoic acid moiety (hereafter called the benzene moiety) and the xanthene moiety, since they are orthogonal to each other.[14] Therefore, it could be acceptable to regard the benzene moiety as the electron donor and the xanthene moiety as the fluorophore (Figure 1B).

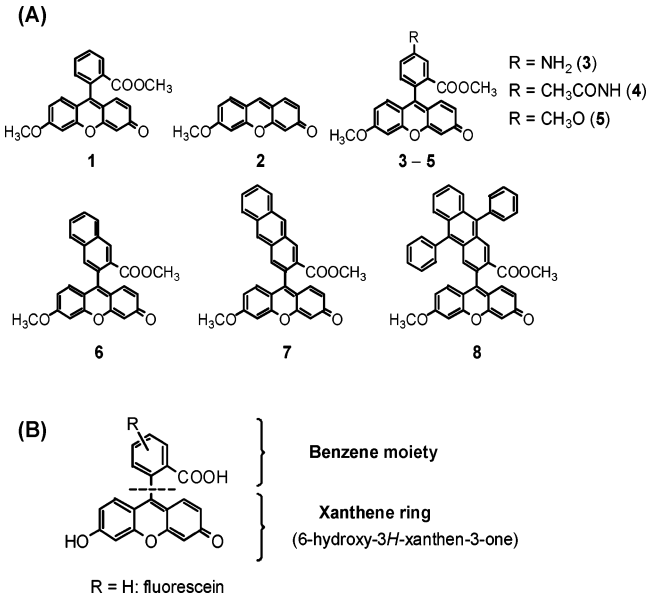

Figure 1. Structures of compounds used in this study: (A) methylated form of fluorescein (**1**), 6-hydroxy-3*H*-xanthen-3-one (**2**), and their benzene ring-substituted derivatives (**3**−**8**). (B) Fluorescein structure was divided into two parts, the benzene moiety and the xanthene ring.

A deoxygenated acetonitrile solution containing **8** (Figure 2A) gives rise, upon a 475 nm laser pulse, to a transient absorption spectrum with maxima at 380, 460, and 700 nm, as shown in Figure 2B.

The absorption band at 700 nm is attributable to diphenylanthracene-2-carboxylic acid (DPA) radical cation, since the one-electron oxidation of DPA by $Ru(bpy)_3^{3+}$ (bpy = 2,2′-bipyridine) yields the radical cation of DPA ($DPA^{\bullet+}$), which exhibits the same absorption band at 700 nm (Figure 2B inset).[15] The absorption band at 460 nm is assigned to the triplet excited state of DPA by comparison with that of authentic ^{3}DPA produced by triplet energy transfer from excited anthracene, as shown in Figure 2C.[16,17] The remaining absorption band at 380 nm is ascribed to the xanthene radical anion ($X^{\bullet-}$), as shown in Figure 2D.[18] Decay of the absorbances at 380, 460, and 700 nm obeyed first-order kinetics with the same rate constant of 1.7 × 10^4 s^{-1}, as shown in Figure 2E,F.

The first-order decay kinetics correspond to the back electron transfer from the $X^{\bullet-}$ to the $DPA^{\bullet+}$ moiety in the radical ion

(12) Parker, C. A.; Rees, W. T. *Analyst* **1960**, *85*, 587−600.

(13) Chen, S.; Nakamura, H.; Tamura, Z. *Chem. Pharm. Bull.* **1979**, *27*, 475−479.
(14) Yamaguchi, K.; Tamura, Z.; Maeda, M. *Acta Crystallogr. C* **1997**, *53*, 284−285.
(15) Fukuzumi, S.; Nakanishi, I.; Tanaka, K. *J. Phys. Chem. A* **1999**, *103*, 11212−11220.
(16) Chattopadhyay, S. K.; Kumar, C. V.; Das, P. K. *Chem. Phys. Lett.* **1983**, *98*, 250−254.
(17) ^{3}DPA was generated by photoirradiation of anthracene (5.0 × 10^{-5} M) with DPA (5.0 × 10^{-5} M) in deaerated acetonitrile at 298 K. T−T absorption spectrum was taken at 50 μs after laser excitation at 355 nm
(18) Compound **2** (50 μM) was photoirraditated in acetonitrile in the presence of *p*-phenylenediamine (1.0 mM) to give the xanthene radical anion (**2**$^{\bullet-}$). The transient absorption spectrum was taken at 298 K at 4.0 μs after laser excitation at 454 nm.

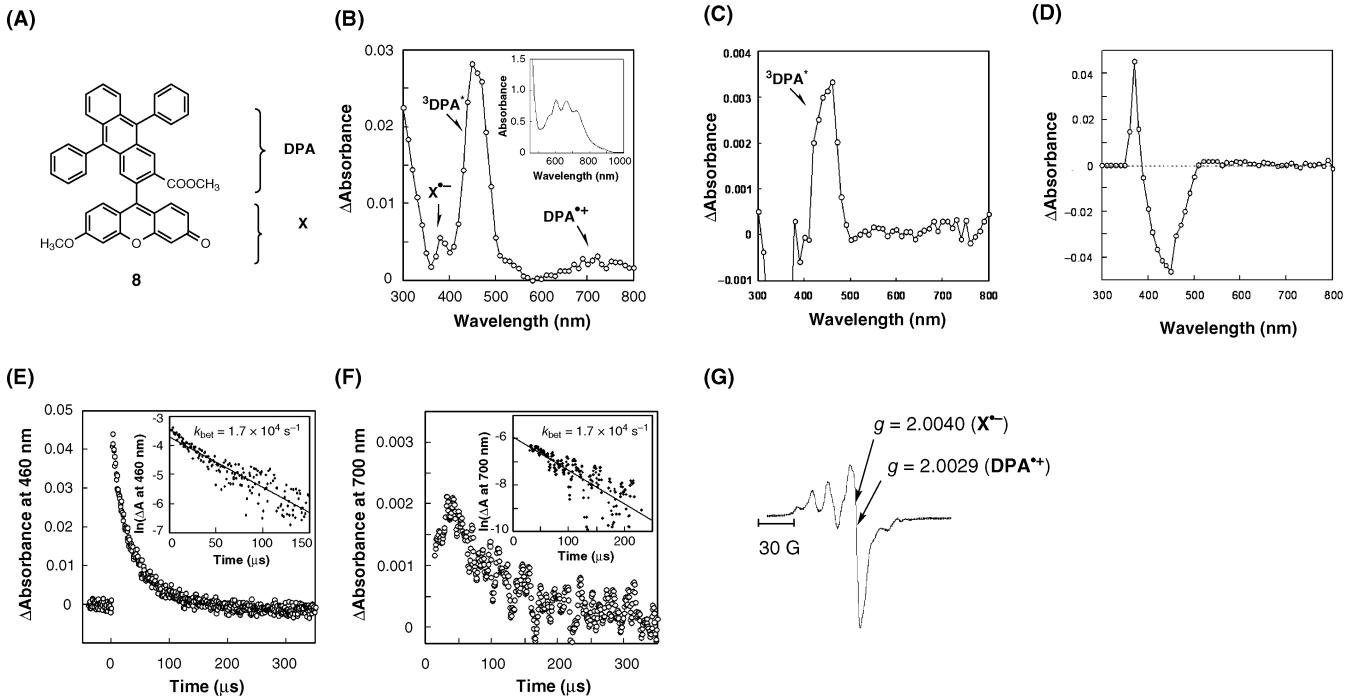

Figure 2. (A) Structure of **8**. (B) Transient absorption spectra of **8** (50 μM) in deaerated acetonitrile at 298 K taken at 14 μs after laser pulse excitation at 475 nm. The visible spectrum of DPA radical cation observed in the reaction of DPA (1.7×10^{-4} M) with $Ru(bpy)_3(PF_6)_3$ (1.7×10^{-4} M) in acetonitrile at 298 K is shown in the inset. (C) T−T absorption spectrum of DPA generated by photoirradiation of anthracene (5.0×10^{-5} M) with DPA (5.0×10^{-5} M) in deaerated acetonitrile at 298 K taken at 50 μs after laser excitation at 355 nm. (D) Transient absorption spectrum observed in the photoreaction of **2** (5.0×10^{-5} M) with *p*-phenylenediamine (1.0×10^{-3} M) in deaerated acetonitrile at 298 K taken at 4.0 μs after laser excitation at 454 nm. (E, F) Decay profiles at (E) 460 nm and (F) 700 nm observed in the photoreaction of **8** after laser excitation at 475 nm. First-order plots are also shown as insets. (G) ESR spectrum measured at 143 K of **8** (1.0×10^{-3} M) under irradiation with light from a high-pressure mercury lamp in frozen acetonitrile.

Table 1. Photochemical Properties of Fluorescein Derivatives

derivative	absorbance maximum (nm)[a]	emission maximum (nm)[a,b]	relative quantum efficiency [b,c]	driving force of electron transfer ($-\Delta G°_{ET}$, eV)	rate constant of electron transfer (k_{ET}, s^{-1}) observed	calculated [f]
1	454, 478	515	0.27	n.d.[e]	*d*	*d*
2	450, 472	500	0.37	*d*	*d*	*d*
3	454, 482	510	0.008	0.91	1.69×10^{10}	1.27×10^{10}
4	456, 480	517	0.21	0.19	1.89×10^{8}	1.38×10^{8}
5	454, 478	516	0.27	0.19	1.03×10^{8}	1.38×10^{8}
6	455, 479	513	0.26	0.25	1.18×10^{8}	3.22×10^{8}
7	454, 483	518	0.01	0.69	3.40×10^{10}	1.18×10^{10}
8	465, 494	516	0.009	0.75	1.11×10^{10}	1.35×10^{10}

[a] Measured in 0.1 M phosphate buffer (pH 7.4). [b] Excited at longer absorbance maximum. [c] Calculated by using fluorescein as a fluorescence standard (ϕ_f 0.85). [d] Not determined. [e] Not detectable. [f] Values were generated from a fit to the Marcus equation. The rate constant of back electron transfer in **8** is also calculated as 1.98×10^4 s^{-1} (observed rate was 1.70×10^4 s^{-1}).

pair, which is in equilibrium with the triplet excited state of DPA, to regenerate the original ground state, because none the derivatives showed any detectable photodegradation, such as dimerization of the anthracene moiety in the case of **8**, under the conditions used.

The rate constants of back electron transfer for other donor−acceptor dyad systems range from 1.6×10^{10} to 9.1×10^3 s^{-1},[19,20] so the value measured for **8** corresponds to a relatively long-lived radical ion pair.

Formation of such a long-lived radical ion pair state of **8** enabled us to obtain the electron spin resonance (ESR) spectrum of the radical ion pair under photoirradiation in acetonitrile at 143 K, as shown in Figure 2G. The ESR spectrum consists of two characteristic signals, of which one is attributable to the radical cation of the diphenylanthracene moiety ($g = 2.0029$) and the other to the radical anion of the fluorophore at a higher g value ($g = 2.0040$), since the authentic $DPA^{\bullet+}$ and $X^{\bullet-}$ gave similar ESR signals of $g = 2.0028$ and 2.0038, respectively.

The rate constant of forward electron transfer (k_{ET}) was calculated by applying eq 1, where ϕ_f and $\phi_f°$ are the quantum efficiencies of fluorescence of a fluorescein derivative and **2** used as the reference compound, respectively, and $k_0 = 1/\tau_0$, where τ_0 denotes the fluorescence lifetime of **2**. The k_0 value was determined as 2.8×10^8 s^{-1} ($\tau_0 = 3.6$ ns). The k_{ET} values are listed in Table 1.

$$\frac{\phi_f°}{\phi_f} = 1 + \frac{k_{ET}}{k_0} \quad (1)$$

The driving force of the back electron transfer ($-\Delta G°_{BET}$ in eV) can be calculated by means of the following equation and

(19) Fukuzumi, S.; Guldi, D. M. In *Electron Transfer in Chemistry*; Balzani, V., Ed.; Wiley-VCH: Weinheim, 2001; Vol. 2, pp 270−337.
(20) Fukuzumi, S.; Ohkubo, K.; Imahori, H.; Shao, J.; Ou, Z.; Zheng, G.; Chen, Y.; Pandey, R. K.; Fujitsuka, M.; Ito, O.; Kadish, K. M. *J. Am. Chem. Soc.* **2001**, *123*, 10676−10683.

Scheme 1

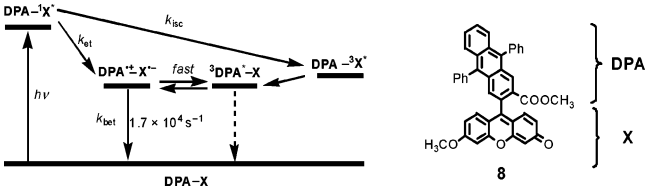

the Rehm−Weller equation (eq 3):

$$-\Delta G^\circ_{BET} = \Delta E_{00} + \Delta G^\circ_{ET} \quad (2)$$

$$\Delta G^\circ_{BET} = e[E^\circ(D^+/D) - E^\circ(A/A^-)] + w_p \quad (3)$$

where e stands for the elementary charge, $E^\circ(D^+/D)$ and $E^\circ(A/A^-)$ are the oxidation potential of the electron donor (methyl benzoate derivative) and the reduction potential of the electron acceptor (**2**, −1.28 V vs SCE), respectively, ΔE_{00} is the singlet excitation energy of the fluorophore (**2**, 2.63 eV), and w_p is the electrostatic interaction energy in the radical ion pair, which corresponds to the work term required to bring the product radical ions to their mean separation in the radical ion pair for the intermolecular electron transfer. If w_p is neglected, then the energy calculated for the charge separation state of **8** (2.60 eV) is significantly higher than the triplet excited state energy of DPA and X (1.81 and 1.94 eV, respectively).[21,22] Since both the radical ion pair and the triplet excited state of DPA are observed in the transient absorption spectrum (Figure 2B), these two states should lie at virtually the same energy levels. For the contact radical ion pairs, the electrostatic interaction energy can be evaluated as $-e^2/4r$ (r denotes the distance between electron donor and acceptor), as reported by Suppan.[23] The r value was estimated as 5 Å by geometry optimization of **8** using DFT calculation. With this value, the w_p value of the radical ion pair derived from **8** is calculated as 0.72 eV. Taking this into account, the energy level of the radical ion pair is obtained as 1.88 eV. This energy level is indeed comparable to that of the triplet excited state of DPA, and the energy diagram of the relaxation pathway of singlet excited compound **8** can be schematically drawn as shown in Scheme 1, in which the charge separation state is located at the lowest energy level, and this firmly supports the aforementioned assignment of the observed rate constant to that of the back electron transfer process.

To verify the importance of w_p in determining the energy level of a radical ion pair in close proximity, relative to the triplet excited state, we synthesized compound **9**, a derivative of **8**, which possesses a longer spacer module between DPA and X (thereby having a larger r value), and examined its decay pathway. The transient absorption spectrum obtained upon irradiation of a solution of **9** in acetonitrile is shown in Figure 3B. The absorption band at 460 nm was attributed to that of the DPA triplet. From the first-order plot of the decay profile measured at 460 nm, the rate constant of the relaxation from the triplet was determined to be 8.6×10^3 s^{-1} (Figure 3C). Thus, we could observe only the absorption band of the triplet excited state of DPA in the laser flash photolysis experiment of **9**.

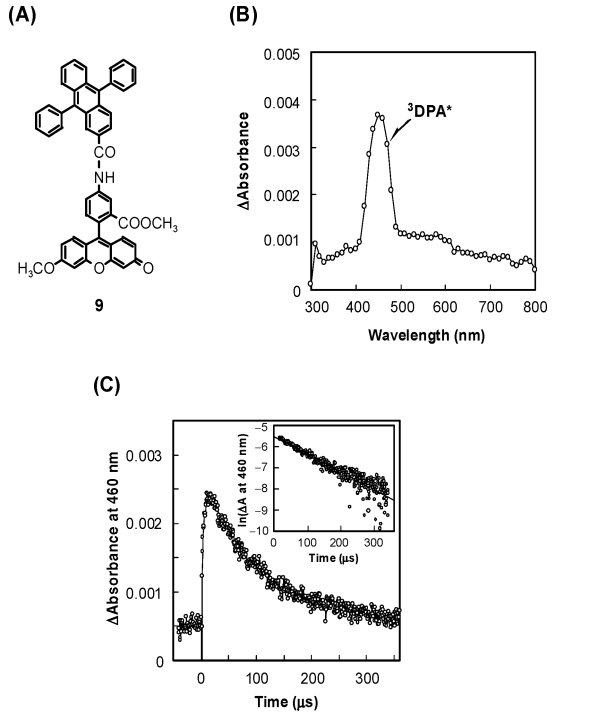

Figure 3. (A) Structure of **9**. (B) Transient absorption spectrum of **9** (5.0×10^{-5} M) in acetonitrile at 298 K taken at 20 μs after laser excitation at 454 nm. (C) Decay profile at 460 nm. Inset: first-order plot.

Scheme 2

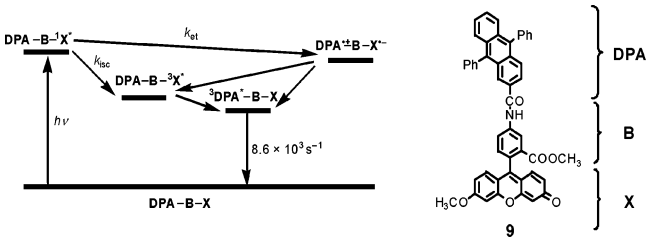

In this case, w_p was calculated from $e^2/\epsilon r$, where ϵ is the dielectric constant of the solvent and r is the distance between the donor and acceptor. In compound **9**, $\epsilon = 38$ and $r = 13$ Å, and w_p was obtained as 0.03 eV. From the Rehm−Weller equation (eq 3), the driving force of the forward electron transfer reaction in **9** was calculated as ∼0 eV, in contrast with the value for directly connected **8** (0.75 eV). Thus, the energy level of the radical ion pair state is much higher than that of the DPA triplet excited state. This can explain the result of the laser flash photolysis experiment for **9**, in which only the triplet state of DPA was observed. The energy diagram of the relaxation pathway of the singlet excited state of **9** can be schematically drawn as shown in Scheme 2.

Similarly, the driving forces of photoinduced electron transfer and back electron transfer were obtained from the one-electron redox potentials of the electron donor and acceptor moieties together with the excitation energy of the singlet excited state of fluorescein derivatives and the w_p values, as listed in Table 1.

Figure 4 reveals a striking parabolic dependence, that is, an increase of the rate constant of photoinduced electron transfer with increasing driving force, but a decrease in the rate constant of back electron transfer in the highly exergonic region.

(21) Kikuchi, K.; Kokubun, H.; Koizumi, M. *Bull. Chem. Soc. Jpn.* **1970**, *43*, 2732−2739.
(22) Shen, T.; Zhao, Z. G.; Yu, Q.; Xu, H. J. *J. Photochem. Photobiol. A* **1989**, *47*, 203-212.
(23) Suppan, P. *J. Chem. Soc., Faraday Trans. 1* **1986**, *82*, 509−511.

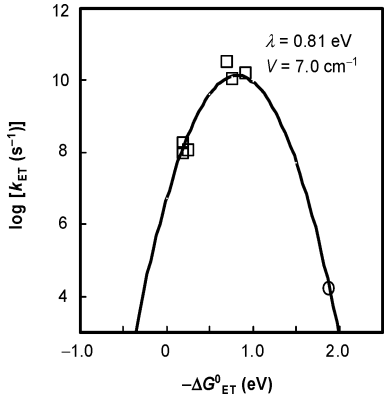

Figure 4. Parabolic dependence of the rate constant of electron transfer (k_{ET}) (squares) and that of back electron transfer for **8** (circle) on the driving force of electron transfer ($-\Delta G°_{ET}$) as predicted from the Marcus theory. The values of $\lambda = 0.81$ eV and $V = 7.0$ cm^{-1} are obtained from the best fit.

To quantify the driving force dependence of the electron transfer rate constants (k_{ET}), the Marcus equation (eq 4) was employed, where V is the electronic coupling matrix element, k_B is the Boltzmann constant, h is the Planck constant, λ is the reorganization energy of electron transfer, and T is the absolute temperature.

$$k_{ET} = \left(\frac{4\pi^3}{h^2\lambda k_B T}\right)^{1/2} V^2 \exp\left[-\frac{(\Delta G°_{ET} + \lambda)^2}{4\lambda k_B T}\right] \qquad (4)$$

By fitting the data in Figure 4 with eq 4, the λ and V values are obtained as $\lambda = 0.81$ eV and $V = 7.0$ cm^{-1} for these fluorescein derivatives.

It should be noted here that the V value (7.0 cm^{-1}) of these fluorescein derivatives, covalently bonded donor−acceptor systems, is relatively small as compared to those of reported dyad systems (∼1−100 cm^{-1}) even though the V term increases exponentially with decreasing distance.[19] This is considered to be a consequence of the characteristic structure of fluorescein derivatives: the carboxylic group of the benzene moiety prevents free rotation around the carbon−carbon bond connecting the benzene ring and the xanthene ring, which are orthogonal to each other. Thus, the electronic coupling between the electron donor (benzene ring) and acceptor (xanthene ring) is quite small, even though they are connected directly. The relative small reorganization energy ($\lambda = 0.81$ eV) can also be explained by the structural uniqueness of the fluorescein molecule. The direct connection of the benzene ring and the xanthene ring excludes intervening molecules of the medium, which would increase the solvent reorganization energy.

Once the Marcus driving force dependence of the rate constants of electron transfer is established, as shown in Figure 4, not only the fluorescence quantum yields of the fluorescein-based fluorescence probes but also the stability of the probes to photoirradiation can be readily predicted from the one-electron oxidation potential of the electron donor moiety of the donor-linked fluorescein molecule. The lower the one-electron oxidation potential, the faster the photoinduced electron transfer in the Marcus normal region in Figure 4, and the lower will be the fluorescence quantum yield. On the other hand, the back electron transfer process from the charge separation state in **8** to the ground state is located deeply in the Marcus inverted region, where the rate constant of electron transfer decreases with increasing driving force of electron transfer ($-\Delta G°_{ET}$). This caused a long-lifetime charge separation state (58 μs) derived from **8**, despite the very close orientation of the radical pair. The faster the back electron transfer, the shorter the lifetime of the reactive radical ion pair, so that less cell damage can be expected, and the stability of the florescence probe may be increased.

Conclusion

In conclusion, the present study has provided for the first time a quantitative basis for rational design of novel fluorescence probes based on the fluorescein platform. Once the Marcus driving force dependence of the rate constants of electron transfer is established, the fluorescence quantum yields of the fluorescein derivatives can be readily predicted, enabling us to attain efficient fluorescence ON/OFF switching with the appropriate reaction site of the probe. Further, the lifetime of the radical ion pair can also be controlled by regulating the back electron transfer rate to avoid undesirable effects on the cell system and instability of the probe.

Acknowledgment. This study was supported in part by the Advanced and Innovational Research Program in Life Sciences from the Ministry of Education, Culture, Sports, Science and Technology, the Japanese Government, by Takeda Science Foundation, and by Nagase Science and Technology Foundation, by research grants from the Ministry of Education, Science, Sports and Culture of Japan (Grant Nos. 12771349, 13557209, and 14030023 to Y.U.), and by a Grant-in-Aid for Scientific Research Priority Area from the Ministry of Education, Science, Culture and Sports, Japan (No. 11228205 to S.F.).

JA035282S